

Quantifying the contribution of white matter microstructure to frequency contrast in gradient echo MRI

Samuel Wharton¹ and Richard Bowtell¹

¹Sir Peter Mansfield Magnetic Resonance Centre, School of Physics and Astronomy, University of Nottingham, Nottingham, United Kingdom

Target audience: Researchers and clinicians interested in the origins of phase contrast in gradient echo (GE) MRI. **Purpose:** Phase images of the human brain acquired at high field strengths using GE-MRI show exquisite tissue contrast. In most studies involving GE phase imaging, it is assumed that the dominant source of phase contrast is the variation in isotropic and anisotropic magnetic susceptibility across different tissues^{1,2}. Recent experiments by Luo *et al.*³, showed a mismatch between the measured internal and external frequencies in a rat optic nerve sample and the values predicted by using a simple isotropic susceptibility model. Luo *et al.* suggested that phase contrast due to NMR-invisible microstructure⁴ could potentially explain this mismatch. In this study, we quantify the contribution of white matter microstructure to the frequency offset in a tissue phantom by using sophisticated simulation techniques to characterise and remove the frequency contribution of bulk isotropic and anisotropic magnetic susceptibility. This approach also yields accurate estimates of the susceptibility (isotropic and anisotropic) of white matter.

Methods: An optic nerve (ON) sample, approximately 20mm long and 4mm in diameter, was harvested from a 60kg pig. The ON sample was placed in a Perspex sphere and surrounded by 1.5 % agarose gel to yield a rigid phantom that was scanned on a Philips 7T whole-body system only 4 hours after harvesting. A dual-echo, 3D, spoiled GE sequence was used to image the spherical tissue phantom with parameters: TR = 28ms; TE₁ = 7 ms; TE₂ = 20ms; scan time = 15 min; isotropic resolution = 0.5 mm; unipolar readout gradients. The tissue phantom was imaged with the optic nerve section oriented at ten different angles to the B₀-field. This resulted in 10 data sets in which the angle, θ , between the nerve axis and B₀ varied between 0 and 90° in steps of ~ 10°. A frequency map was formed at each sampling orientation by calculating the difference in the phase of the two echoes of the dual-echo data. The measured frequency maps were then high-pass filtered using the SHARP method⁵ and co-registered to a common sample space. Binary masks of the ON samples were hand drawn on magnitude data. Based on these masks, the frequency perturbation maps due to a continuous bulk isotropic magnetic susceptibility offset, χ_I , relative to the surrounding agarose gel and to a cylindrically symmetric anisotropic magnetic susceptibility⁶, χ_A , associated with the ON sample were simulated using fast Fourier methods⁶ for each θ -value. In these simulations, the values of χ_A and χ_I were set to unity. For the anisotropic susceptibility simulations, the principle component of the tensor was aligned with the fiber direction in the ON sample (i.e. along the main axis of the cylindrical nerve). The simulated frequency maps were fitted to the measured frequency data by estimating the values of χ_I and χ_A that minimised the least-squares error in voxels external to the ON sample (i.e. in the agarose gel surrounding the ON sample) for the frequency data associated with all θ -values. This approach is advantageous, since by focusing on the external field perturbation it eliminates any sensitivity to microstructure effects which only produce signal changes within the sample. The composite frequency maps created with the best-fitting χ_I and χ_A values were then subtracted from the measured frequency data to yield residual frequency maps at each sampling orientation which represent the measured frequency offsets that are poorly explained by the bulk isotropic and anisotropic susceptibility effects.

Results: The best-fitting χ_I and χ_A values based on the external frequency variation in the measured data, f , (1st row in Fig. 1) were found to be -81.52 ± 0.06 ppb and 11.28 ± 0.09 ppb, respectively. Maps of the simulated frequency, f_{sim} , generated using the fitted χ_I and χ_A values are also shown in Fig. 1 (2nd row), along with the maps of the variation of the residual frequency offset, $f_R = f - f_{sim}$ (3rd row). Fig. 2 shows a plot of the average f_R value inside the ON sample at each θ -value. The variation in f_R is well characterised by a fit of the form $f_R = A \sin^2 \theta + b$, with coefficients $A = -5.59 \pm 0.07$ Hz and $b = 4.88 \pm 0.12$ Hz.

Discussion: The careful design of this experiment allowed the bulk isotropic and anisotropic susceptibility of a fresh WM sample to be determined from external field measurements, independent of local effects of microstructure. The fitted value for χ_I (-82 ppb) is close to the value determined by Luo *et al.*³ in a rat ON sample (-116 ppb) and adds to the growing body of evidence suggesting that WM is diamagnetic relative to water. The fitted magnitude of χ_A (11 ppb) is of the same sign, but slightly larger than the 8 ppb value estimated by Lee *et al.*⁷, who applied a similar approach to a fixed, post-mortem human WM sample. The average residual frequency offset inside the optic nerve decreased by 5.59 Hz as the nerve orientation was rotated from parallel to perpendicular to the field, showing a $\sin^2 \theta$ dependence on the angle of the nerve to the field, which is consistent with the predicted effect of WM microstructure^{4,6}. The θ -independent frequency component ($b=4.88$ Hz) may contain contributions from both microstructure and exchange processes⁸ and its origin needs further investigation.

Conclusion: WM microstructure induces significant fiber-orientation dependent frequency offsets that need to be accounted for in *in-vivo* studies of the human brain which utilise high-field GE-MRI phase images. The effect of these offsets on quantitative susceptibility maps is of particular interest.

References: 1. Duyn *et al.* 2007. PNAS. 104:11796–11801. 2. Liu *et al.* 2010. MRM. 63:1471-1477. 3. Luo *et al.* 2013. MRM. DOI: 10.1002/mrm.24762. 4. He and Yablonskiy. 2009. PNAS 106:13558-13563. 5. Schweser *et al.* 2010. Neuroimage. 54:2789-2807. 6. Wharton and Bowtell. 2012. PNAS. 109:18559-18564. 7. Lee *et al.* 2010. PNAS. 107:5130-5135. 8. Zhong *et al.* 2009. Neuroimage. 40:1561-1566.

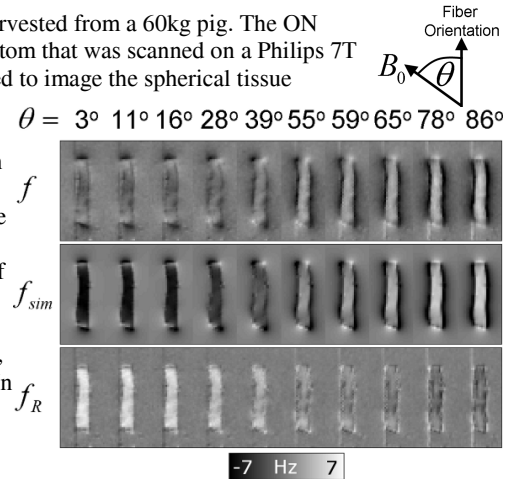


Fig. 1 – Representative maps of measured (f), simulated (f_{sim}), and residual (f_R) frequency at each θ value.

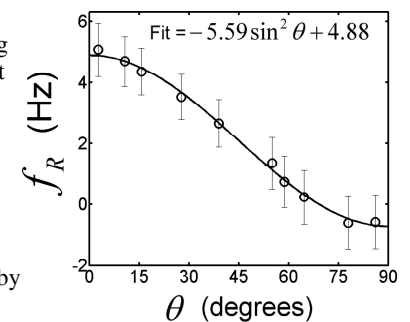


Fig. 2 – Variation with θ of the average residual frequency offset inside the ON sample. Errors = pooled standard deviation.